Comparative study of ferromagnetic superconductors ($Ru_{1-x}Nb_xSr_2Eu_{1.4}Ce_{0.6}Cu_2O_{10}$) by different preparation methods

M.E. Botello-Zubiate, C. Santillán, O.E. Ayala-Valenzuela, and J.A. Matute-Aquino

Abstract

Polycrystalline ferromagnetic superconducting samples of rutheno-cuprates with chemical formula $Ru_{1-x}Nb_xSr_2Eu_{1.4}Ce_{0.6}Cu_2O_{10-\delta}$ (x = 0, 0.2, 0.4, 0.6, 0.8 and 1) were prepared by two different routes. An almost pure Ru-1222 type phase with a small amount of the Ru-2116 or Ru-1212 phases in some of the samples were determined. Randomly oriented particles in laminates form with a length and width of a few micrometers together with agglomerates were observed. Particle size distributions, average particle sizes porosity and final density depends on the processing route. Critical magnetic fields, intra- and inter-grain transition temperatures are functions of sample composition and processing route.

Keywords: Ferromagnetic superconductors, resistance; critical magnetic fields.

Introduction

Since the discovery of the ferromagnetic and superconducting rutheno-cuprates $RuSr_2RCu_2O_8$ (Ru-1212) and $RuSr_2(RCe)_2Cu_2O_{10-\delta}$ (Ru-1222) where R = Gd or Eu numerous studies have been made to clarify the origin of the magnetic ordering without reaching a definitive conclusion [1,2,3]. The Ru-1222 type rutheno-cuprates with formula $(Ru_{1-x}Nb_x)\ Sr_2Eu_{1.4}Ce_{0.6}Cu_2O_{10-\delta}$, with a strong bidimensional character in their crystalline structure and with competitive ferromagnetic and antiferromagnetic interactions, is an ideal system to study the origin of the magnetic and superconducting ordering mechanisms. It is so because the dilution of the spin system, with the addition

of Nb^{+5} ion, which does not has magnetic moment and has a radio similar to Ru^{+5} , would allow us to study in detail how the gradual coupling process between the magnetic moments occurs. Additionally, the total substitution of Nb by Ru (Nb-1222) maintains the crystal structure and conserves the superconductivity. Here we present a comparative study of the influence of different processing routes (agate mortar milling -series 1-against planetary ball milling-series 2-) on the phase composition, microstructure and magneto-transport properties.

Experimental

Processing: Nominal compositions were prepared starting from high purity oxide powders (≥90.9%) of RuO_2, Nb_2O_3, Eu_2O_3, CeO_2, $SrCO_3$ and CuO, previously dried at 100°C during 24 hours. The starting oxides were meticulously mixed and milled in an agate mortar (series 1) and using a planetary ball mill (serie 2) and then they were calcined in a three steps heat treatment procedure: 24 hours at 1000, 1020 and 1040°C respectively, with intermediate millings between heat treatments and using heating and cooling rates of 5 and 3°C/min respectively. Finally, the samples were synthesized at 1075°C during 24 hours under oxygen atmosphere with heating and cooling ramps of 3 and 0.5°C/min respectively [3,4]

Characterization: The X-ray diffraction patterns were measured at room temperature in a Phillips diffractometer model X'pert MPD with Cu-Kα radiation (λ=1.5406 Å) and with an angular step of 0.02° in an angular interval from 20 to 120°. The X-ray diffraction patterns were refined by the Rietveld method using the Fullproof program [5] for the determination of phases composition, lattice parameters and others crystallographic parameters. The microstructure was observed in scanning electron

microscopes JEOL model JSM-5800 LV and JEOL model JSM-7401F and chemical elemental analysis was carried out with energy-dispersive systems EDAX S60/DX90 and Oxford 350X. The particle size was determined with a Mastersizer light scattering analyzer and with scanning electron microscopy. Resistance vs Temperature curves for different applied magnetic fields were measured in a Quantum Design Physical Properties Measurement System.

Results and discussion

Figure 1 shows the evolution of phase formation for the sample x=0 (series 1) after the three intermediate heat treatments and final sintering followed by the changes of the X-ray diffraction patterns. It can be observed a intensity diminution of some peaks (for example at 2θ=38.8° and 28.8°) and a intensity increase in some other peaks (for example at 2θ=30.7, 41.8, 44.3 and 54.6°) as the three heat treatments are realized. The X-ray diffraction pattern after sintering at 1075°C during 24 hours shows well-defined peaks corresponding to the Ru-1222 phase completely formed.

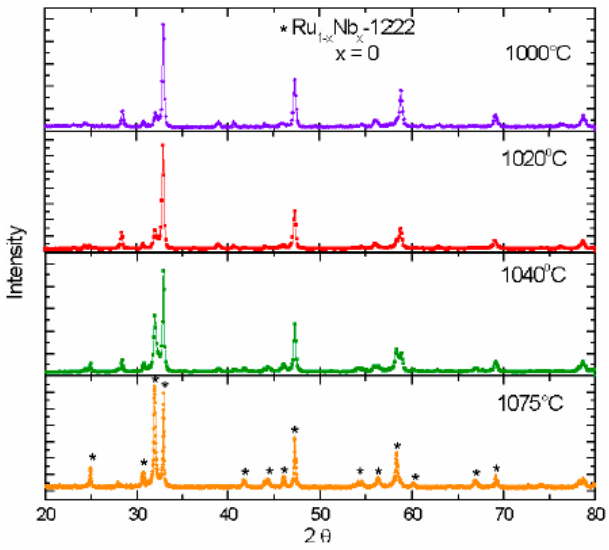

FIGURE 1. XRD patterns after intermediate heat treatments and final sintering of $RuSr_2Eu_{1.4}Ce_{0.6}Cu_2O_{10-\delta}$.

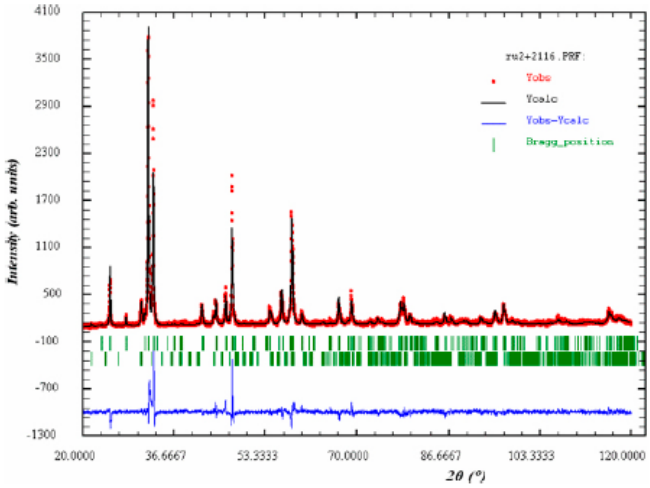

FIGURE 2. Rietveld refinement of the X-ray diffraction pattern corresponding to the x=0.2 sample.

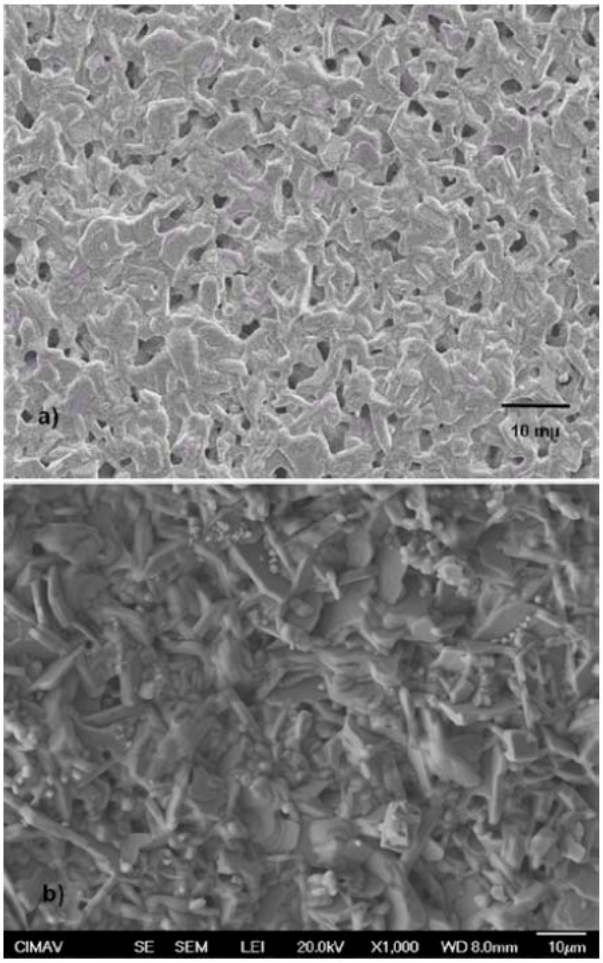

FIGURE 3. Scanning electron microscopy images of the samples $RuSr_2Eu_{1.4}Ce_{0.6}Cu_2O_{10}$ of the series 1 (Fig. 3a) and series 2 (Fig. 3b).

Figure 2 shows the Rietveld refinement of the X-ray diffraction pattern corresponding to the x =.2 sample (series 1). For all compositions of this series the Rietveld refinement was carried out for the tetragonal Ru-1222 type structure (space group I4/mmm) as the main crystallographic phase, for the composition with x=0 we obtained small amounts of the Ru-2116 type phase (group P21/n) and Ru- 1212 type phase (P4/mbm) For the samples with x= 0.2 to x=0.8 only we obtained small amounts of the Ru-2116 type phase (~2-5%). The lattice parameters obtained for the sample with x=0 were a=3.835 Å and c=28.500 Å, this lattice parameters increase with addition of Nb, which is in correspondence with the higher ionic radio of Nb ($r_{ionic}\ ^{+5}_{Ru}$ = 0.65Å, $r_{ionic}\ ^{+5}_{Nb}$= 0.64 Å), these results are in agreement with previous data [6]

TABLE I. Critical superconducting temperatures for composition x=0, series 1 and 2.

Parameters	Series 1				Series 2			
Composition (x)	0	0.4	0.6	1	0	0.4	0.6	1
Onset transition temperature (K) (T_{onset})	46	43	38	6	47	28	30	23
Intra-grain transition temperature (K) (T_1)	40	35	33	-	40	23	22	17
Inter-grain transition temperature (K) (T_2)	34	30	30	-	30			
R=0 Ω transition temperature (K) ($T_{R=0}$)	30	26	27	-	23	16	17	8

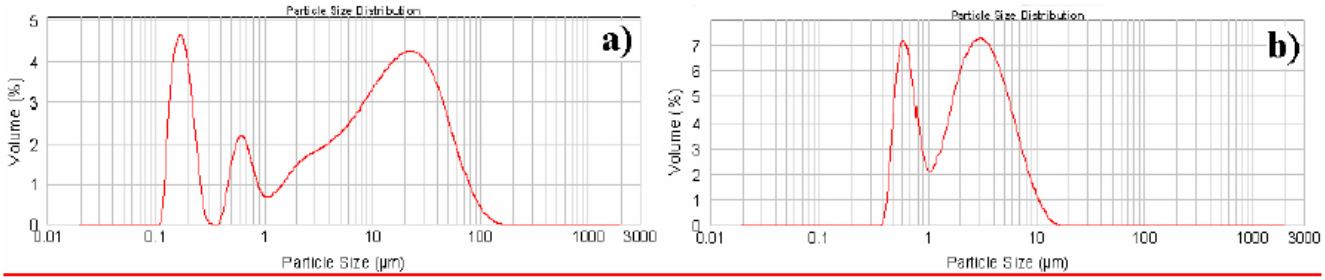

FIGURE 4. Volume percent vs. particle size shows three-modal and bi-modal distributions for series 1 (Fig. a) and series 2 (Fig. b).

Figure 3a and 3b show scanning electron microscopy images of the samples $RuSr_2Eu_{1.4}Ce_{0.6}Cu_2O_{10}$ for the series 1 and 2 respectively. Particles in laminates form

are observed randomly oriented with a size between 2-3 μm, together with agglomerates and some porosity. The porosity is greater for series 1 than for series 2, which is in correspondence with a higher calculated density for series 2. After sintering the final average density were 75.5 g/cm^3 and 85.2 g/cm^3 for the series 1 and series 2 respectively. A similar morphology was observed in all compositions of the series.

Volume percent versus particle size shows three-modal and bi-modal distributions for composition x=0 of series 1 and 2 respectively after the third heat treatment see Fig. 4. Series 2 shows a narrower particle size distribution than series 1 and a smaller average particle size than series 1 Average particle sizes of 8.52 and 2.36 μm were determined for series 1 and 2 respectively. These results suggest that the planetary ball mill route produces a better particle size distribution and average particle size than the agate mortar route.

From the electrical resistance versus temperature curves for different static applied magnetic fields four different critical temperatures could be determined: the onset transition temperature $T_{onset,}$ the intra-grain transition temperature T_1, the inter-grain transition temperature T_2 and the R=0 Ω transition temperature $T_{R=0}$. The onset transition temperature is the higher temperature when the resistance begins to fall during the superconducting transition, the intra-grain (intergrain) transition temperature is the temperature associated to the to the establishment of the superconducting state inside the grains (in the grain boundaries) and the R=0 Ω transition temperature is the temperature associated to the establishment of the superconducting state in the whole material. Figure 5 shows electrical resistance versus temperature and derivative curves for different static applied magnetic fields for sample compositions x = 0, 0.4, 0.6 and 1.

Figure 5a for series 1 show that resistance R=0 Ω was reached for compositions x=0, 0.4 and 0.6 for all static applied magnetic fields. This means that the critical magnetic field is beyond 15 T. But the sample with x=1 does not reach the zero resistance condition even for the lowest measured temperature. On the other side, Fig. 5c for series 2 show that resistance R=0 Ω was reached for sample with x=0 for all applied magnetic fields, while for compositions x=0.4, 0.6 and 1 the resistance R=0 Ω was only obtained for applied magnetic fields until 5 T. Table I show the different critical temperatures for composition x=0 for series 1 and 2. From this table one can observes higher critical temperatures for series 1 than for series 2. Additionally, for series 2 only one maximum in the derivatives could be determined.

For series 1 with compositions x = 0.4 and 0.6 the onset transition temperatures are 43 and 38 K and they reach zero resistance at 26 and 27 K respectively. For composition x=1 of this series one can observes an important diminution of the onset temperature to 6K but it does not reach the zero resistance temperature even for the lowest measured temperature. On the other side, for series 2 with compositions x=0.4 and 0.6 the onset transition temperatures are 28 and 30 K and they reach zero resistance at 16 and 17 K respectively. For composition x=1 of this series an onset transition temperature of 23 K and a zero resistance temperature of 8 were determined. From the table and the data presented above we can conclude that the superconducting transition temperatures of both series are not significantly affected by Nb substitution in the RuO_2 layers in this system, with exception of the samples with composition x=1.

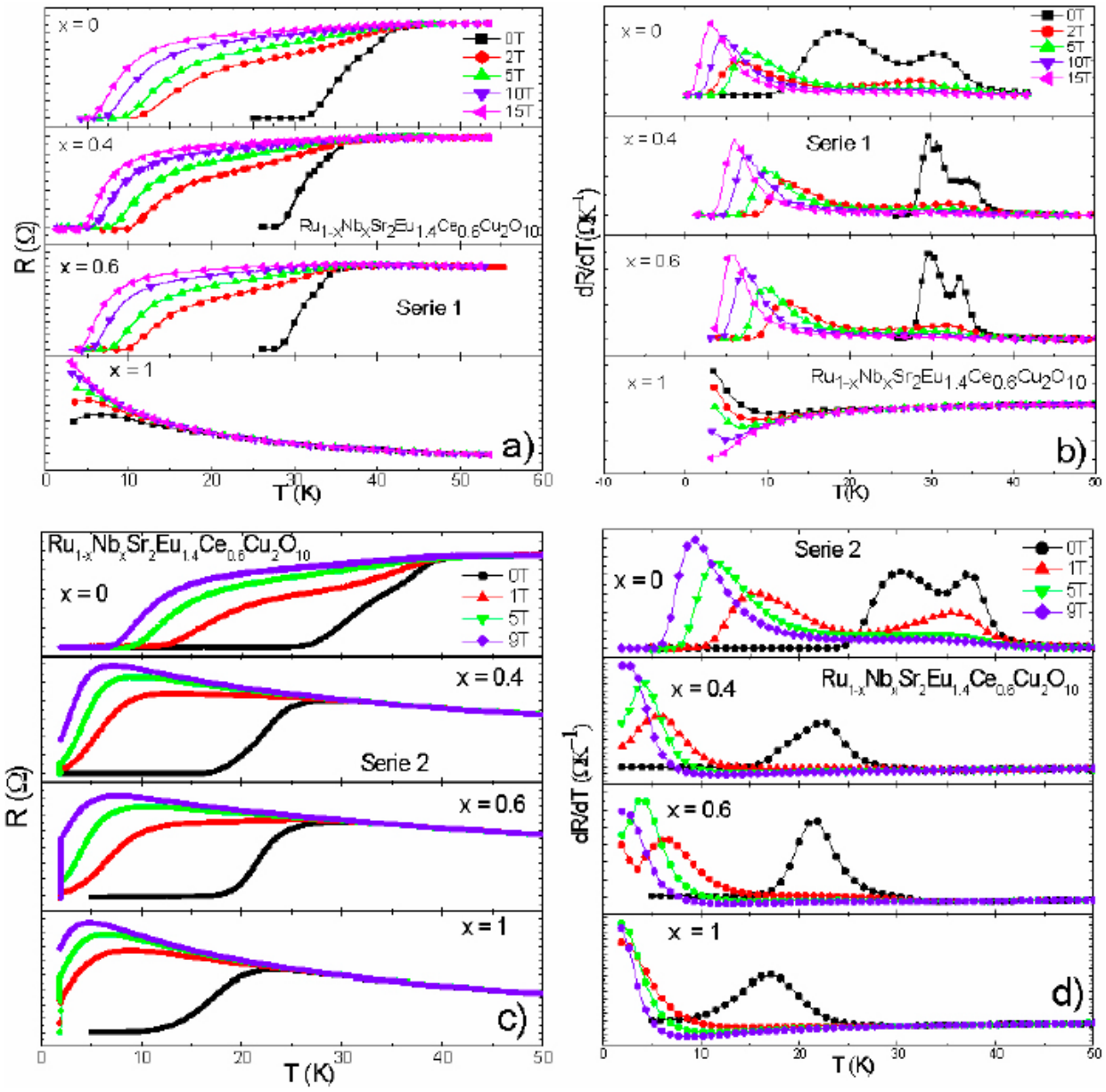

FIGURE 5. Resistance vs. Temperature curves for different static applied magnetic fields to samples with x = 0, 0.4, 0.6 and 1 (Figs. 5a and 5c) and its derivates curves (Figs. 5b and 5c).

Conclusions

The $Ru_{1-x}\,Nb_x\,Sr_2\,Eu_{1.4}\,Ce_{0.6}\,Cu_2O_{10-\delta}$ (x=0, 0.2, 0.4, 0.6, 0.8 and 1) system prepared by agate mortar (series 1) and planetary ball mill (series 2) show an almost pure Ru-1222 type phase with small amounts of Ru-2116 or Ru-1212 phases. A microstructure of randomly oriented particles in laminates form with a length and width

of a few micrometers together with agglomerates was determined. Series 2 has smaller porosity, higher density, smaller average particle size and narrower particle size distribution than series 1. However, series 1 has higher critical temperatures than series 2. Lower limits of 15, 9 and 5 T for critical magnetic fields as well as onset temperatures, intra- and inter-grain temperatures and zero resistance temperatures were determined for different compositions in both series.

Acknowledgment

The authors (MEB, JMA) would like to thank the NHMFL for its help in PPMS measurements (series 1) and CONACyT by its support to this work (CONACyT Project 60687: Superconductividad y ferromagnetismo en las cer´amicas que contienen rutenio: origen de la frustraci´on magn´etica en un Sistema de baja dimensionalidad)

References

1. W. Lynn, Y. Chen, Q. Hang, S.K. Goh, and G.V.M. Williams, Physical Review. B 76 (2007) 014519.
2. R. Lal et al., Journal of Physics: Condensed Matter 18 (2006) 2563.
3. S. García, I. Ghivelder, S. Soriano, and I. Felner, The Europian Phsycal Journal B (2006) 307.
4. V.P.S. Awana, H. Kishan, E. Takayama-Muromachi, and A.V. Narlikar, Modern Physics Letters B 20 (2006) 1901.
5. Rodriguez-Carvajal, FULLPROOF: A Rietveld refinement and pattern matching analysis program On line.
6. H.K. Lee and G.V.M. Williams Physica C 41 (2004) 172.